IEEE Access
Multidisciplinary ⋮ Rapid Review ⋮ Open Access Journal

Received 21 July 2022, accepted 3 August 2022, date of publication 10 August 2022, date of current version 18 August 2022.

Digital Object Identifier 10.1109/ACCESS.2022.3197894

RESEARCH ARTICLE

Dynamic Online Grid Impedance Estimation and Its Effects on DC Capacitor Lifetime in Variable Frequency Drive

RAMESH PANDURANGAN[1], PALANISAMY KALIANNAN[2], (Senior Member, IEEE), AND PARAMASIVAM SHANMUGAM[3], (Senior Member, IEEE)

[1]School of Electrical Engineering, Vellore Institute of Technology, Vellore 632014, India
[2]Department of Energy and Power Electronics, Vellore Institute of Technology, Vellore 632014, India
[3]ESAB India Ltd., Chennai 600058, India

Corresponding author: Ramesh Pandurangan (prameshchennaicbe@gmail.com)

ABSTRACT Grid impedance plays a significant role in the performance and design considerations of nonlinear devices like Variable Frequency Drive (VFD). VFD operates across domestic, industrial, and residential applications under different grid configurations and capacities including renewables. IEEE 519 standard recommends grid short circuit ratio and thereby grid impedance as an index for the individual and overall current harmonic performance of the connected utilities. This research investigation details a comprehensive approach for an online dynamic grid impedance estimation and may also give an insight into the hardware implementation within a VFD to achieve optimum performance and reliability during installation. A VFD of 250 kW is used for real-time measurements and simulation with varying grid configurations to determine grid impedance and lifetime of the DC capacitors. A fuzzy model is developed based on the established knowledge base for the estimation of the grid impedance of a generic grid. The fuzzy model is further enhanced to estimate the lifetime of the DC capacitor.

INDEX TERMS AC-DC power converters, impedance estimation, total harmonic distortion, variable speed drives.

I. INTRODUCTION

VFDs are widely used in domestic and industrial applications where motors serve as prime movers. These motors when driven through VFD offer energy saving, productivity, and maintenance enhancements, due to their operational load characteristics. IEEE 519 recommends guidelines of current distortion limits [1] as a percentage of load current (I_L) at PCC, indexed to the corresponding grid short circuit ratio (R_{sce}). Grid short circuit capability is also defined as the ratio of maximum short circuit current (I_{sc}) and maximum demand load current (I_L) at the point of common coupling (PCC). On the other hand, IEC 61000-3-2 and IEC 61000-3-12 recommend guidelines on current emission limits by nonlinear loads like VFD as a function of grid short circuit ratio (R_{sce}) [2], [3]. A detailed understanding of grid impedance is important to establish the reliability of VFD. Online sine current injection for measurement of power system line impedance through network analyzer to establish the wideband characteristics of resistance and inductance of every conductor is discussed [4]. A sinusoidal current of high frequency is injected into the grid from the PWM converter, and grid impedance is determined from the measured response in terms of magnitude, the phase angle of injected current, and resulting voltage [5]. Few research papers propose grid impedance estimation through a recursive least square algorithm in the existing power converter and introduce eventual disturbances when estimation falls below the quality threshold, validated through experimental testing [6]. Frequency-dependent grid impedance determination through injection of PWM signals via simple hardware is discussed [7]. A single or double harmonic current frequency injection from the grid-connected inverter through harmonic voltage addition, to an inverter reference voltage for

The associate editor coordinating the review of this manuscript and approving it for publication was Md Mejbaul Haque.

grid impedance estimation using suitable algorithms, is discussed [8]. Non-parametric grid impedance estimation by injection of current impulse from the grid-connected inverter and performing DFT analysis of impulse response is discussed [9]. Frequency-dependent grid impedance variation within the fundamental cycle due to the connected power converters switching behavior and its impact on network harmonic impedance is discussed [10]. Determination of grid impedance in wide frequency range by monofrequent current injection from hysteresis controlled PWM converter onto low voltage public network are analyzed [11]. Dynamic grid impedance measurement through decoupled control of grid-connected inverter in typical micro grid application is discussed [12]. This paper investigates and proposes an online grid impedance measurement as a built-in solution for niche product ranges making use of existing VFD hardware and software platforms, unlike other earlier research work. This research details the measurement, and analytical evaluation of grid short circuit current (I_{sc}), and grid impedance (Z_{TH}) offline. An insight of proposed built-in hardware and software changes to monitor VFD input current, and voltage and thereby estimate dynamic online grid impedance is one of the significant outcomes. Estimation of DC capacitor lifetime with suitable built-in temperature sensors to monitor their performance and reliability may also support the implementation of an intelligent IoT platform. This investigation may add value to the VFD manufacturer's niche product design.

This paper is organized per research activities as follows:

1) Grid impedance analytical evaluation and measurement results with various types of grid configuration are detailed (a 250 kW VFD is considered in this investigation).
2) Different grid impedance measurements and estimation proposals were discussed.
3) Harmonic current distortion and relevant standards fulfillment is discussed.
4) Modeling and simulation, proposed hardware inclusions within VFD for dynamic online grid impedance measurement are detailed.
5) DC capacitor lifetime estimation is studied.
6) Fuzzy model development for grid impedance and capacitor lifetime is realized.

Research investigation is inferred in subsequent sections and consolidated in the Conclusion.

II. GRID IMPEDANCE AND HARMONIC PERFORMANCE

Limits for harmonic currents are recommended in several international standards. IEEE 519 does not recommend the limits for individual equipment, but overall, for the customer. Recommendation by standards is to ensure customers/equipment, limit harmonic injection onto the utility grid thus maintaining voltage distortion of the system voltage within acceptable norms. Grid short circuit ratio (R_{sce}) is also detailed in terms of permissible individual harmonic current and total harmonic current distortion. The total demand load constitutes the current drawn linear and non-linear loads. At an industrial site, the PCC is in general the connectivity point between non-linear and other loads. Grid short circuit ratio (R_{sce}) also supports determining grid impedance (Z_{TH}). IEEE 519 defines general rules for evaluating harmonic limits at an industrial installation [1]. Grid capability is often considered at the load interface point in terms of short circuit ratio. Grid short circuit (R_{sce}) of the network is expressed as the ratio of short circuit apparent power (S_{sc}) at PCC and VFD rated apparent power (S_{VFD}). Grid impedance (Z_{TH}) is thus expressed simply as the ratio of source voltage (Vs) and short circuit current (I_{sc}).

III. GRID IMPEDANCE AND GRID CONFIGURATION

In this investigation, a 250 kW VFD is connected to different grid configurations of typical industrial applications. This supports grid impedance evaluation from simulated, estimated, and measured results.

A. INDUSTRIAL GRID AND CONFIGURATIONS

Typical product approval and qualification test center comprise three test bays (A, B, and C), providing a combination of six grids (Sample 1: Grid 1 – 6) as in Fig 1, 2, and 3. 11 kV Grid serves as a source of power for these test bays which is further step down to nominal voltage through 2500 kVA, 1000 kVA, and 500 kVA transformers respectively. Motors of these test bays operate both in motoring and regenerative quadrant enabling loading of 250 kW test VFD at 50 % and 100 % output capacity respectively. A 12 pulse standalone transformer was (1 MVA) additionally interconnected at the input of 250 kW VFD in 400 kW and 800 kW test bays (Grid 2 and 4 configurations). Input voltage and current measurements were done both at idle and loaded conditions (50 % and 100 %) using Power Quality Recorder PQ Box 200. Additionally current and voltage distortion was also measured.

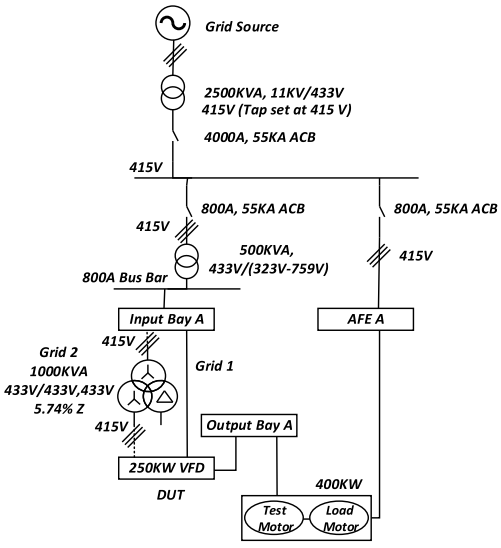

FIGURE 1. Single line diagram of 250 kW VFD in 400 kW test system (GRID 1 and GRID 2: 12 Pulse, 1 MVA Transformer) (Method A, B).

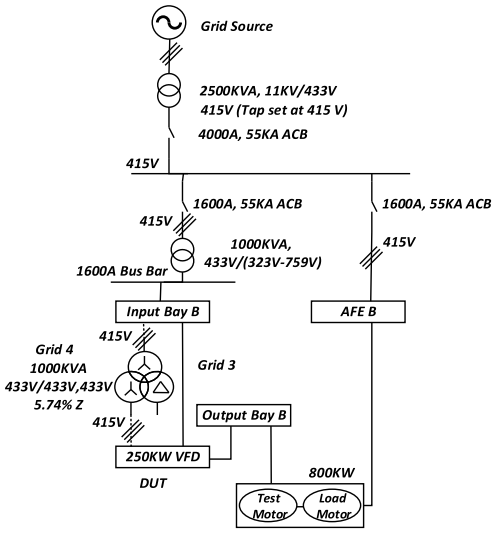

FIGURE 2. Single line diagram of 250 kW VFD in 800 kW test system (GRID 3 and GRID 4: 12Pulse, 1 MVA Transformer) (Method A, B).

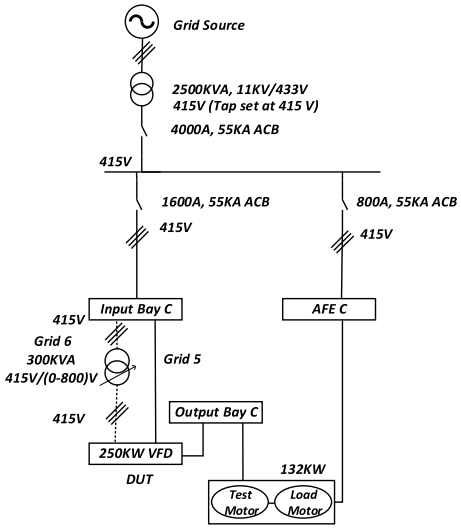

FIGURE 3. Single line diagram of 250 kW VFD in 132 kW test system (GRID 5 (Direct) and GRID 6: 300 kVA) (Method A, B).

A comprehensive study with analysis was performed to estimate and measure the grid impedance, and grid short circuit capability.

B. INDUSTRIAL GRID AND CONFIGURATION

An additional analysis of the above grid configuration with continuous measurement of input voltage, current, and harmonic distortion (Sample 2) using PQ Analyzer Hioki was performed as in Fig 4. Analytical evaluation of grid impedance and short circuit capability was consolidated.

IV. GRID IMPEDANCE EVALUATION

A. GRID IMPEDANCE ESTIMATION (METHOD A)

Fault current can be estimated stepwise as below:

1) Representation of electrical system (Grid 1 - 6) as a single line diagram (SLD) with all sources of short circuit current included.

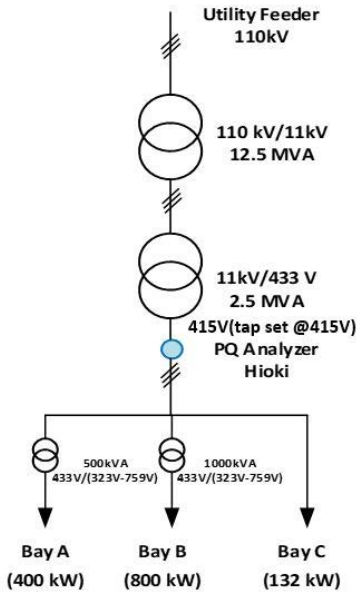

FIGURE 4. Single line diagram of Grid impedance estimation (Method C).

2) Circuit components are also included in SLD.
3) Impedances of system components represented in SLD.
4) Impedance values of transformers, bus ways, cables, etc. can be referred to from manufacturer data [13].
5) Current limiting devices are eliminated during short circuit calculations and replaced with copper bus bars.
6) Point-to-Point calculation method supports the accurate determination of short circuit current. This method considers either unlimited primary short circuit current or limited primary current as per design.

Grid impedance (Z_{TH}) is estimated as the ratio of source voltage (Vs) and short circuit current (I_{sc}) calculated stage-wise as per SLD. Detailed Point-to-Point procedures and expressions of short circuit current estimation for a three-phase system are detailed in [13].

B. GRID IMPEDANCE ESTIMATION (METHOD B)

Due to the increased use of nonlinear devices across applications network harmonic / line impedance can also be defined as a parallel combination of both grid / upstream impedance and connected device / downstream impedance at any connection point. Network harmonic impedance at any load connection point is established by injecting current at a frequency that is not available in the grid. Voltage measurements before and after the current injection are recorded. Line impedance is thus defined as the ratio of the difference between voltages (before and after current injection) and injected current [14]. An offline method of determining grid impedance and short circuit current through practical measurement is discussed. In this investigation, grid impedance is measured with the load in disconnected mode. METREL 3144 [15] is used for the measurement of grid impedance (Z_{TH}) as shown in

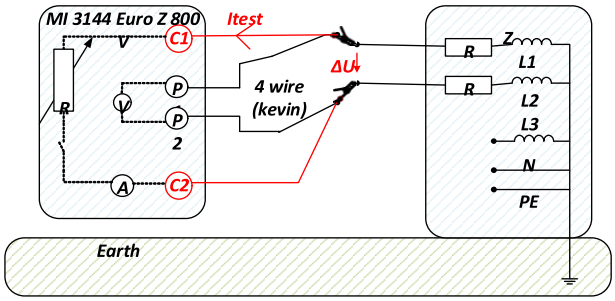

FIGURE 5. Line or Grid impedance measurement (Method B).

FIGURE 6. Grid impedance measurement set-up (METREL 3144).

Fig. 5 and 6. High current impulses are injected into the system at the point of load connectivity through METREL. Synchronous sampling is the measurement principle. Line / Grid impedance is the impedance determined within the current loop when a short circuit situation persists. The internal shunt resistor is connected across C1 and C2 for a half-cycle period to measure the current (I_{test}) (2). Voltmeter (across P1 and P2) measures both voltages with no load (V_{unload}) and loaded (V_{load}) conditions. Impedance Z_{TH} is determined as the ratio of the voltage difference between load and unloaded condition and the current (I_{test}) as in (1).

$$Z_{TH} = \frac{(V_{unloaded} - V_{loaded})}{(I_{test})} = \frac{\Delta V}{I_{test}} \tag{1}$$

$$I_{test} = \frac{(V_{ac})}{(Test\_load + R\_leads + R\_int)} \tag{2}$$

where V_{ac} = test voltage (40V . . . 800V) at 415 V;
$Test\_load$ = percentage of equivalent load resistance;
R_leads = C1 and C2 test lead resistance;
R_int = internal resistance/impedance of power source

Prospective current (I_{psc}) / (I_{sc}) displayed is expressed by (3)

$$I_{psc} = \frac{(V_n * k_{sc})}{Z_{TH}} \tag{3}$$

where Z_{TH} = measured grid impedance;
V_n = nominal source voltage;
k_{sc} = Correction factor (I_{sc} factor) for I_{psc}

C. GRID IMPEDANCE ESTIMATION (METHOD C)

Grid impedance of the connected load can also be estimated from both current and voltage measurements at the grid connectivity point during operation. Grid impedance (Z_{TH}) is estimated as the ratio of voltage and current difference under the loaded and unloaded conditions as shown in (4).

$$Z_{TH} = \frac{(V_{unload} - V_{load})}{(I_{load} - I_{unload})} = \frac{\Delta V}{\Delta I} \tag{4}$$

where (I_{load}) is the current drawn by the load. Unload current (I_{unload}) is significantly less than nominal current and hence not considered during grid impedance estimation. This procedure of online grid impedance estimation is not dependent on grid short circuit current (I_{sc}).

An uncontrolled six pulse VFD of 250 kW, 415 V, and 420 A rating was tested in grid configurations (Sample 1), and impedance was determined using Method A and Method B. Analytical evaluation of short circuit fault currents at different downstream stages of test bays (A, B and C) with various grid configurations (Sample 1) is represented in Single line diagram as in Fig. 7. Short circuit current, grid impedance, and X/R ratio of test bays (A, B, and C) through analytical evaluation (Method A) are consolidated in Table 1.

TABLE 1. Analytical evaluation of grid parameters in test bays (Sample 1) (Method A).

Operating Conditions/ Grid configuration (at 415V)	I_{sc} (kA) (VFD Input)	Z_{TH} (VFD Input)	X/R ratio
BAY A /GRID 1	4.9 kA	84.7 mΩ	2.76
BAY A (12P) / GRID 2	2.4 kA	173 mΩ	3.59
BAY B / GRID 3	10.2 kA	40.7 mΩ	3.16
BAY B (12P) / GRID 4	4.0 kA	104 mΩ	4.79
BAY C (Direct) / GRID 5	14.0 kA	29.6 mΩ	1.89
BAY C (300 kVA) / GRID 6	2.1 kA	197 mΩ	1.23

Measured grid parameters in test bays (Method B) are consolidated in Table 2.

It is observed (Sample 2) grid impedance from practical measurements by Method C (V_{unload} = 240$V_{L\text{-}N}$, V_{load} = 234 $V_{L\text{-}N}$, I_{load} = 530A) was at 11 mΩ as against the estimated value of 10.5 mΩ highlighted (short circuit current kA) in Fig. 7 and expressed by (5), using Method A respectively.

$$Z_{TH} = \frac{V_n}{I_{sc}} = \frac{415}{41.74} = 10\ m\Omega \tag{5}$$

From the above example, it is evident that grid impedance estimation and measurements by Method A/B/C are in-line with close tolerance.

V. EXPERIMENTAL TESTING AND RESULTS

Motor load setup in a typical product qualification center as shown in Fig. 8 is utilized for experimental testing. The outcome of this testing fulfills the research objective and grid

TABLE 2. Measurement of grid parameters in test bays (Sample 1) (Method B).

Operating Conditions/ Grid configuration	I_{sc} (kA) (VFD Input)	Z_{TH} (VFD Input)	X/R ratio
BAY A @415V / GRID 1	5.4 kA	76.9 mΩ	2.94
BAY A @ 415 V (12P) / GRID 2	2.6 kA	159.6 mΩ	3.64
BAY B @415V / GRID 3	9.2 kA	45.2 mΩ	3.80
BAY B @ 415V (12P) / GRID 4	4.3 kA	96.5 mΩ	4.80
BAY C @ 415V (Direct) / GRID 5	15.4 kA	26.9 mΩ	1.61
BAY C @ 415V (300 kVA) / GRID 6	1.9 kA	218.4 mΩ	1.26

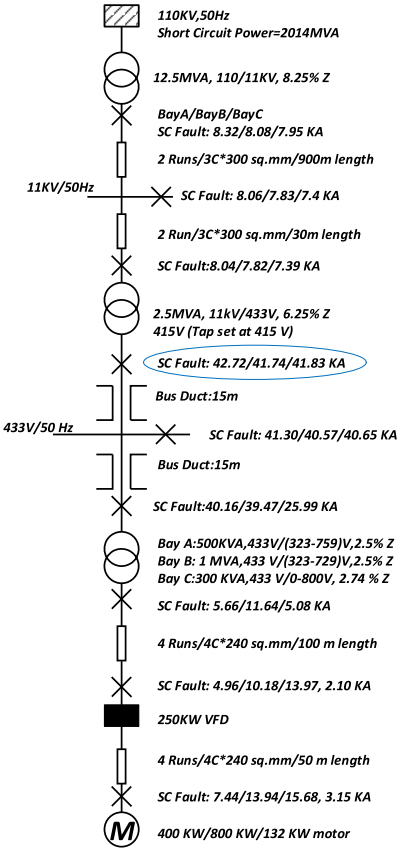

FIGURE 7. Single line diagram of Test Bays A, B, and C with short circuit currents (Grid 1,3,5 and 6).

impedance estimation by Method C. VFD is connected to the test motor of the regenerative motor load system as shown in Fig. 8. Output of 500/1000/2500 kVA transformer is set as per input voltage requirements of 250 kW VFD connected to test motors in test bays A/B/C. A regenerative test system comprises of back to back coupled load and test motors of identical capacity. Power Analyzer and DPO are connected to measure voltage, current, distortion at VFD input, and DC

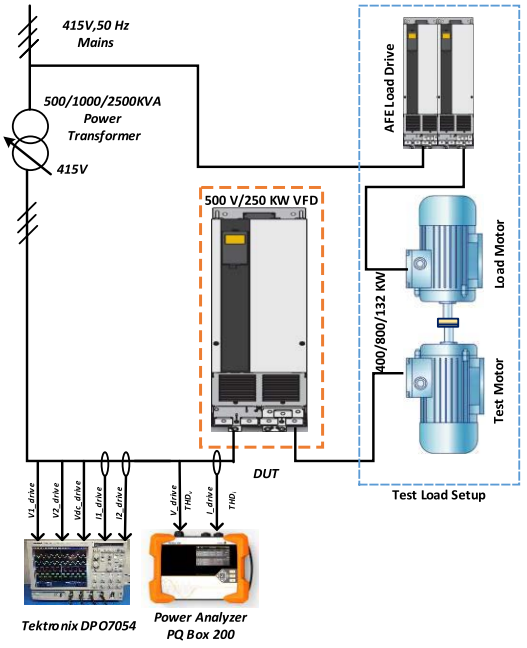

(a)

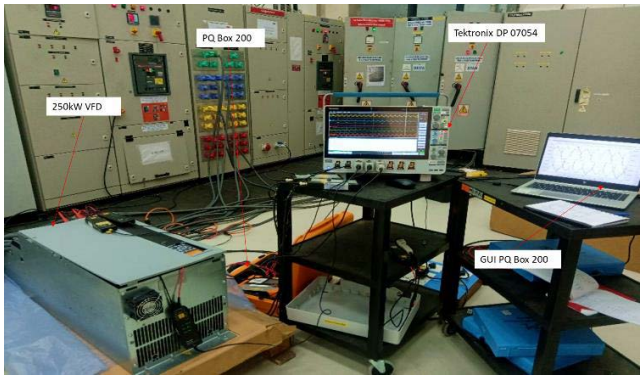

(b)

FIGURE 8. (a) Block diagram of test system (b) Experimental set-up.

capacitor voltage. A balanced 415V power supply to VFD is ensured through suitable tap change/adjustments at the secondary output of 2500/1000/500/300 kVA transformers considered in this research investigation.

Following measurements were done with various grid configurations as below and test results are consolidated:

1) A 250 kW VFD (6 pulse) loaded at 50% (132 kW) and 100% (250 kW) capacity in Bay A (Grid 1) and Bay B (Grid 3) respectively (Sample 1).
2) A 1MVA 12 pulse (star winding output) transformer is interfaced in addition to the existing 500 kVA and 1 MVA transformer in Grid 2 and Grid 4 (Sample 1) configuration enabling testing of 250 kW VFD.
3) A VFD of 250 kW is powered with a 415V balanced direct supply (2500 kVA) in Bay C (Grid 5) and in addition, though 300 kVA transformer source (Grid 6) loaded to a maximum of 132 kW capacity (Sample 1).

A. RESULTS

Grid impedance estimation (Method C) of various grid configurations (Sample 1) is supported by the measurement of VFD input voltage, and current, and consolidated in Table 3. It is observed when VFD is connected to Grid 5 with high short circuit current capability (Table 2) THD_i (49.1%) and VFD max current value (404 A) are significant (Table 4). VFD input THD_i, and max current value increase are directly proportionate observed during measurements. Table 4 and Fig. 13 provide an overview of grid impedance impact on VFD input THD_i, THD_v, and RMS/Max current spectrum.

TABLE 3. Measurement results of VFD input voltage and current in test bays with various grid configuration (Sample 1).

Grid configuration	V_{unload} (V) L-L	V_{load} (V) L-L	I_{load} (A)	Z_{TH} (mΩ) (Method C)
BAY A (132 kW) / GRID 1	416	409	196	61.8
BAY A (250 kW) / GRID 1	416	400	366	75.7
BAY A (250 kW/12P) / GRID 2	416	387	388	129.5
BAY B (132 kW) / GRID 3	413	408	202	42.8
BAY B (250 kW) / GRID 3	413	404	369	46.9
BAY B (250 kW/12P) / GRID 4	413	393	379	91.3
BAY C (132 kW) (Direct) / GRID 5	414	411	209	24.8
BAY C (132 kW) (300 kVA) / GRID6	414	390	207	200.8

TABLE 4. Measurement results of VFD input THDi and THDv of test bays with various grid configuration (Sample 1).

Grid configuration	Input *THDv*	Input *THDi*	Input current (A/RMS)	Input current (A/Max)
BAY A (132 kW) / GRID 1	5.9%	36.9%	196	351
BAY A (250 kW) / GRID 1	9.4%	28.6%	366	608
BAY A (250 kW/12P) / GRID 2	13.8%	24.3%	388	561
BAY B (132 kW) / GRID 3	4.9%	39.4%	202	374
BAY B (250 kW) / GRID 3	7.6%	30.8%	369	609
BAY B (250 kW/12P) / GRID 4	12.5%	25.3%	379	588
BAY C (132 kW) (Direct) / GRID 5	2.3%	49.1%	209	404
BAY C (132 kW) (300 kVA) / GRID6	11.3%	28.2%	207	333
132 kW/100 kA GRID *	1.2%	74%	259	510
250 kW/100 kA GRID *	1.6%	47.2%	430	748

* Simulated Grid results

VI. SIMULATION AND RESULTS

A simulation model for a 250 kW VFD is developed in MATLAB® Simulink. Estimated and measured grid impedance, and short circuit current (kA) as shown in Table 1 and Table 2 are considered in the modeling. However, the X/R ratio of the downstream transformers in Fig.1-3 is considered to be 7. VFD DC-Link capacitor (C_{dc}) and inductor (L_{dc}) effective values are 78 μH and 11750 μF as shown in Fig. 9 are considered in the modeling. Resistive load (R_L) is considered for simulation and adjusted to match VFD input measured current values for various grid configurations and loading conditions. The active (R_S) and reactive (L_S (X_S)) components of grid impedance are represented in the equivalent circuit of VFD as shown in Fig. 9. Table 5 provides a comprehensive overview of simulation results. Grid impedance estimated using Method C and simulation values are in close agreement as shown in Table 5. VFD input current distortion and Max current values are observed significantly increased among grid configurations with lower impedance values and highest short circuit current capability both during measurements and simulation. Simulation results of the 100 kA capability grid are observed to have the highest

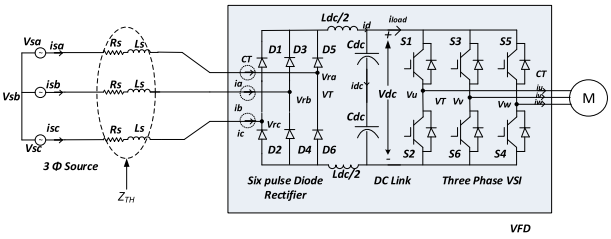

FIGURE 9. Equivalent circuit of VFD: Grid Impedance, Current, and Voltage sensors.

TABLE 5. Simulation results of VFD input voltage and current with different grid configuration (Sample 1).

Grid Configuration	V_{unload} (V) L-L	V_{load} (V) L-L	I_{load} (A) L-L	Z_{TH} (mΩ) (Method C)	Z_{TH} (mΩ) (Sim)
B AY A (132 kW) / GRID 1	415	405	204	84.9	84.7
BAY A (250 kW) / GRID 1	415	394	381	95.4	84.7
BAY A (250 kW/12P) / GRID 2	415	385	372	139.7	173
BAY B (132 kW) / GRID 3	415	410	213	40.6	40.7
BAY B (250 kW) / GRID 3	415	404	418	45.6	40.7
BAY B (250 kW/12P) / GRID 4	415	392	413	96.5	104
BAY C (132 kW) (Direct) / GRID 5	415	412	207	25.2	29.6
BAY C (132 kW) (300 kVA) / GRID 6	415	392	206	193.4	197
*132 kW/100 kA GRID	415	414	259	6.68	4.15
*250 kW/100 kA GRID	415	414	430	4.02	4.15

* Measurements were done on Grid 1- 6 / Bay A, B and C
* 100 kA Grid is considered during simulation only

impact on VFD input current distortion (47.2%) and max current (748 A) as shown in Table 4. It is observed that measurements, simulation, and analytical observations of grid parameters through Method A/B/C are in close agreement with identical grid configurations (Sample 1) during this research analysis.

VII. IMPLEMENTATION OF GRID IMPEDANCE ESTIMATION AND MEASUREMENTS IN VARIABLE FREQUENCY DRIVE

Grid impedance is an important parameter in the determination of VFD dynamic performance. A simple offline, and dynamic online measurement with an estimation model of grid impedance is discussed. Grid impedance has a significant impact on the current distortion of the connected VFD. Distortion limits are recommended in IEEE 519, IEEE 61000-3-2, and IEEE 61000-3-12.

A. PROPOSAL 1

Online Grid impedance measurement and estimation with the use of built-in VFD hardware in niche products are discussed in detail and its equivalent circuit is shown in Fig. 9. In most of the high featured VFDs available in the market, current and voltage sensors are adapted in the input circuit apart from the output stage. These sensors are in general based on Hall effect phenomena with galvanically isolated primary and secondary design. These types of sensors use the ''True RMS'' algorithm which can accurately measure distorted AC waveforms in VFD applications. Closed-loop magnetic sensors for current measurements are also used on the output side of VFD. With grid impedance changing dynamically in industrial sites, VFDs are subjected to considerable current stress. This increased current distortion impacts the lifetime reduction of DC capacitors in VFD. Current (i_a, i_b, i_c) and voltage sensors (v_{ra}, v_{rb}, v_{rc}) at the input of VFD in general handle voltage unbalance, phase loss, and power factor estimation. A noninvasive online method of impedance estimation with methodology, algorithm, measurement uncertainty, and verification of results is detailed in earlier research work [16]. This estimation methodology serves as the basis for this research proposal with the use of suitable built-in hardware and software as briefed. Dynamic online grid impedance measurement and estimation using Method C are considered in this proposal.

Following are the inputs for grid impedance measurements, estimation, and determination:

1) With VFD powered ON and in the idle state, the unloaded parameters are (V_{unload}, I_{unload}) measured with built-in sensors. Once the VFD is loaded, the load parameters V_{load} and I_{load} are monitored. Once these parameters are fetched, the grid impedance estimation is done using expression (4).

2) Additionally, with VFD in operation, continuous change of V_{load}, I_{load}(present values) and their measurements can also support dynamic online grid impedance estimation to a reasonable accuracy as shown in (6).

$$Z_{TH} = \Delta V / \Delta I \tag{6}$$

where ΔV is the difference between V_{unload} and present load voltage, and ΔI is the difference between I_{unload} and present load current. Linear regression on several such measurement points of V and I under loaded conditions gives much accurate determination of grid impedance [20].

3) Estimation of grid impedance (active/R and reactive/X components) through FFT (fast Fourier transform) of VFD input voltage and current components at the desired frequency is considered. Dynamic online impedance measurement and estimation using discrete Fourier transformation in typical micro grid applications [12] serves as a good reference for resolving resistance and inductance components of grid impedance. Verification of this proposal using Method C was done through MATLAB simulation using typical grid impedance values which were measured and simulated (Table 3, 4 and Table 5).

4) VFD in general comprises both motor control and application processors. Measurements, calculation, and estimation of power, distortion, and protection features are synthesized with suitable control algorithms in the application processor, as a niche product is designed with voltage and current sensors as shown in Fig. 9.

B. PROPOSAL 2 (FUZZY MODEL)

A simple fuzzy model has been realized for grid impedance verification and estimation (Table 7). Fuzzy rules were formed based on the analytical correlation between the set of input ($V_{unload}, V_{load}, I_{load}, I_{unload}$) and output parameters ($Z_{TH}, X/R$). As V_{unload} is stable in grids considered in this investigation and I_{unload} is insignificant compared to I_{load}, unloaded parameters are considered constant during fuzzy rule formation. The membership functions for input and output parameters are defined by fuzzy linguistic variables and applicable ranges as consolidated in Table 6.

The membership function plots (Input variable Gaussian membership function for V_{load}, I_{load}, and output triangular membership function for Z_{TH}, X/R) were realized using the MATLAB fuzzy software module. Rule base consisting of IF-THEN condition statement for six rules with two inputs (load voltage and load current) and two outputs (grid impedance and X/R ratio) were considered. Six test conditions/rules on measured/estimated data are consolidated along with relevant fuzzy rules in Table 7. Fuzzy output is realized for the defined rules using the max-min compositional process [17]. Among several available Defuzzification techniques, Centroid of Area (COA) is considered in this investigation to compute the numeric fuzzy output from the fuzzy interface system as shown in Fig. 10. Surface plots for grid impedance (Z_{TH}) and X/R ratio are also predicted in MATLAB. The root mean square error (RMSE), the fraction of variance (R^2), accuracy of the fuzzy model (A), predicted fuzzy value (F), measured/estimated value (M), the number of test conditions (N), rate of error (e_i), defuzzified value

TABLE 6. Estimated input and output parameters with linguistic variables and rules for fuzzy model (Sample 1).

Test conditions /Rule	V_{load} (V) (Input)	I_{load} (A/RMS) (Input)	Z_{TH} (mΩ) (Method C) (Output)	X/R (Output)
BAY A (132 kW) / GRID 1	M(405)	VL(204)	M(84.9)	M(2.76)
BAY A (250 kW) / GRID 1	L(394)	M(381)	H(95.4)	M(2.76)
BAY B (132 kW) / GRID 3	H(408)	VL(202)	L(42.8)	H(3.16)
BAY B (250 kW) / GRID 3	M(404)	H(418)	L(45.6)	H(3.16)
BAY C (132 kW) (Direct) / GRID 5	VH (411)	VL(209)	VL(24.8)	L(1.89)
BAY C (132 kW) (300 kVA) / GRID6	VL (392)	VL(206)	VH(193.4)	VL(1.23)

* IF STATEMENT FOR INPUT PARAMETERS and THEN STATEMENT FOR OUTPUT RESPONSE
* Linguistic Variables: VL (Very Low), L (Low), M (Medium), H (High), and VH (Very High)
* 100 kA grid simulation is not considered for grid impedance fuzzy

TABLE 7. Fuzzy logic model error and accuracy for grid impedance and X/R (Sample 1).

Test conditions /Rule	Z_{TH} (X/R) (Est.)	Z_{TH} (X/R) (Fuzzy)	Error % Z_{TH} (X/R)	Accuracy % Z_{TH} (X/R)
BAY A (132 kW) / GRID 1	84.9(2.76)	74.3(2.59)	12.5(6.2)	87.5(94)
BAY A (250 kW) / GRID 1	95.4(2.76)	125(2.6)	31.2(5.8)	68.8(94.2)
BAY B (132 kW) / GRID 3	42.8(3.16)	54.2(2.77)	16.6(12)	83.4(88)
BAY B (250 kW) / GRID 3	45.6(3.16)	55.5(3)	21.7(5.1)	78.3(95)
BAY C (132 kW) (Direct) / GRID 5	24.8(1.89)	34.4(2)	38.7(5.8)	61.3(94.2)
BAY C (132 kW) (300 kVA) / GRID6	193.4(1.2)	154(1.49)	20.4(24)	79.6(76)

*100 kA grid simulation is considered for capacitor lifetime fuzzy

TABLE 8. Performance of fuzzy logic model (Sample 1).

Fuzzy Output	RMSE	R^2	A (%)
Grid Impedance (Z_{TH})	21.927	0.98834	78.5
X/R ratio	0.234	0.998427	90.2

as expressed in (1-5) of [17] is used to predict the performance of grid impedance fuzzy model with respect to estimated/measured values (Table 7, Table 8).

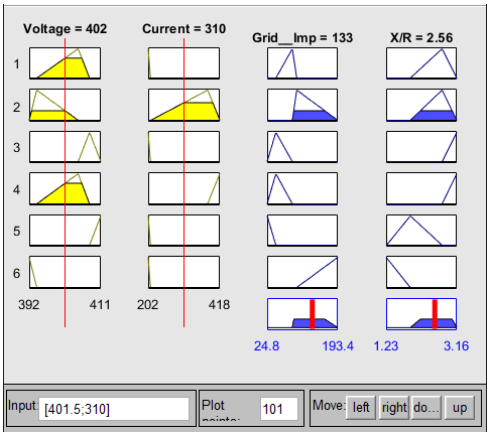

FIGURE 10. Fuzzy Rule Interface: Grid impedance.

VIII. ESTIMATION OF DC CAPACITOR LIFETIME

The Lifetime (L_x) of a DC capacitor in hours is expressed by (7). Estimation is done using relevant parameters, manufacturer recommendations [19], and simulated harmonic current spectrum as expressed by (19) – (21) in [18] for various grid configurations and load conditions.

$$L_x = L_0 * 2^{\frac{(T_0 - T_x)}{10}} * 2^{\frac{(\Delta T_0 - \Delta T_x)}{K}} * \left(\frac{V_0}{V_x}\right)^{4.4} \tag{7}$$

where *Vo* and *Vx* are DC capacitor specified and actual voltage values. Ambient and internal hotspot temperatures with variations during operation (T_o, ΔT_o) and (T_x, ΔT_x) are considered accordingly. Fig. 14 summarizes in detail the estimated DC capacitor lifetime of different grid configurations with measured grid impedance as per Table 2.

A. IMPACT OF DC CAPACITOR LIFETIME

Grid impedance causes a significant impact on RMS current spectrum and distortion at VFD input. From the consolidated simulation results in Table 12, a 250 kW VFD in a 100 kA grid has the highest DC capacitor fundamental (184 A) and harmonic current (22.2 A) contribution. DC capacitor lifetime in this grid configuration is reduced significantly (64873 hours) due to the least grid impedance (4.15 mΩ) compared to other configuration and loading conditions considered in this investigation. Lower the value of grid impedance, increase in capacitor losses (P_d), internal hot-spot temperature (ΔT_x), and harmonic current spectrum are inevitable. Electrolytic capacitors have always been the weakest link in the design of VFD. Adequate sizing of DC capacitors in terms of total capacitance value (based on ripple content analysis), and suitable DC link design configuration can be explored by VFD design engineers for establishing good reliability [21]. Alternatively, an AC reactor or Passive Harmonic Filter addition at the input of VFD can provide better harmonic mitigation and ripple reduction. Manufacturers have also sought alternative capacitor technology implementation like film capacitors.

B. FUZZY MODEL

A simple fuzzy model has been realized for capacitor lifetime verification and estimation. Fuzzy rules were formed based on the analytical correlation between the set of input (V_{load}, I_{load}, Tx) and output parameters (ΔTx, Lifetime in hours). The membership functions for input and output parameters are defined by fuzzy linguistic variables and applicable ranges as consolidated in Table 9. Among several available Defuzzification techniques, Centroid of Area (COA) is considered in this investigation to compute the numeric fuzzy output from the fuzzy interface system as shown in Fig. 11. Various critical fuzzy parameters as expressed in (1-5) of [17] is used to predict the performance of Capacitor lifetime fuzzy model with respect to estimated/measured values (Table 10 and Table 11).

TABLE 9. Estimated input and output parameters with linguistic variables and rules for fuzzy model (Sample 1).

Test Condition/ Rule	V_{load} (V) (Input)	I_{load} (A/RMS) (Input)	Op.Temp (T_x) (Input)	Temp Rise (ΔT_x) (Output)	Capacitor Lifteime (kHrs) (Output)
Bay A / G1 (132 kW)	M(405)	VL(204)	L(60)	L(0.44)	VH(1.128)
Bay A / G1 (250 kW)	L(394)	M(381)	H(69)	L(0.46)	VH(1.127)
Bay B / G3 (132 kW)	H(408)	VL(202)	L(60)	M(0.93)	H(1.091)
Bay B / G3 (250 kW)	M(404)	H(418)	VH(72)	H(1.12)	H(1.077)
Bay C / G5 (132 kW: D)	VH(411)	VL(209)	L(60)	H(1.49)	M(1.049)
Bay C (132 kW :300 kVA) / G6	L(392)	VL(206)	L(60)	VL(0.08)	VH(1.157)
(132 kW:100 kA GRID)	L(390)	M(259)	M(64)	VH(7.98)	L(0.670)
(250 kW:100 kA GRID)	VL(387)	VH(430)	VH(75)	VH(8.44)	VL(0.649)

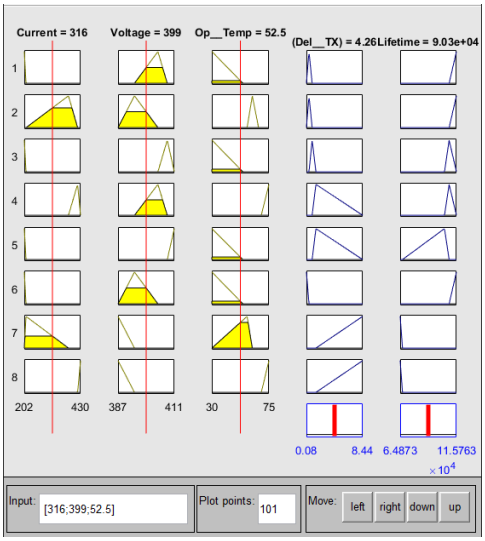

FIGURE 11. Fuzzy Rule Interface: Capacitor Lifetime.

The critical output parameters of the above fuzzy models which justify the objective of this research investigation are grid impedance and capacitor lifetime. Temperature sensors mounted on the hotspot area of a DC capacitor during the product qualification process can monitor internal

TABLE 10. Performance of fuzzy logic model (Sample 1).

Fuzzy Output	RMSE	R^2	A (%)
Temperature rise (ΔT_x)	0.478	0.9959	62.2
Capacitor Lifetime	0.176	0.9951	85.4

TABLE 11. Fuzzy logic model error and accuracy for capacitor lifetime and temperature rise (ΔT_x) (Sample 1).

Test conditions /Rule	Lifetime kHrs(10^5) (ΔT_x) (Est.)	Lifetime kHrs(10^5) (ΔT_x) (Fuzzy)	Error % Lifetime (ΔT_x)	Accuracy % Lifetime (ΔT_x)
BAY A (132 kW) / GRID 1	1.128 (0.44)	0.903 (0.785)	19.9(78.5)	81.1(21.5)
BAY A (250 kW) / GRID 1	1.127 (0.46)	0.903 (0.785)	19.8(70.6)	81.2(29.4)
BAY B (132 kW) / GRID 3	1.091 (0.93)	0.903 (0.785)	17.2(15.6)	82.8(84.4)
BAY B (250 kW) / GRID 3	1.077 (1.12)	1.10 (1.19)	2.1(6.25)	97.9(93.8)
BAY C (132 kW) (Direct) / GRID 5	1.049 (1.49)	0.903 (0.785)	13.9(47.3)	86.1(52.7)
BAY C (132 kW) (300 kVA) / GRID6	1.157 (0.08)	0.903 (0.785)	21.9(78.1)	78.1(21.9)
132 kW: 100 kA GRID	0.670 (7.98)	0.825 (7.31)	23.1 (8.39)	76.9 (91.6)
250 kW: 100kA GRID	0.649 (8.44)	0.654 (8.81)	0.77 (4.38)	99.2 (95.6)

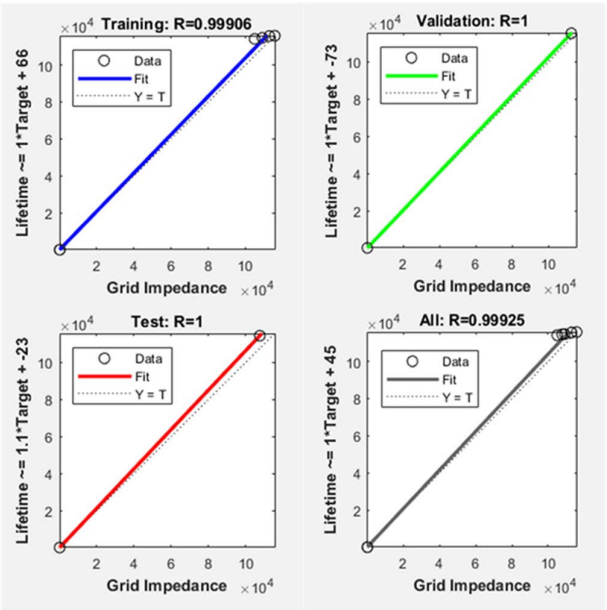

FIGURE 12. Predictive model : Performance Regression Plot (Grid Impedance versus Capacitor Lifetime).

TABLE 12. DC capacitor lifetime estimation with different grid configuration and DC capacitor current.

Grid Configuration	Lifetime (Hours)	Grid impedance (mΩ)	DC Capacitor Fund/Harmonic current (A)
Bay A / G1 (132 kW)	112885	84.7	41/7.1
Bay A / G1 (250 kW)	112754	84.7	42/9.5
Bay A / G2 (250 kW:12P)	114134	173	32/10.5
Bay B / G3 (132 kW)	109166	40.7	61/10.3
Bay B / G3 (250 kW)	107722	40.7	67/11.0
Bay B / G4 (250 kW: 12 P)	111605	104	49/10.6
Bay C / G5 (132 kW: D)	104968	29.6	77/12.8
Bay C (132 kW : 300kVA) / G6	115763	197	17/6.0
(132 kW:100 kA GRID)	66961	4.15	178/21.0
(250 kW:100 kA GRID)	64873	4.15	184/22.2

temperature rise (ΔT_x) and also support reliability and lifetime estimation (7).

Grid impedance has a direct impact on VFD capacitor lifetime from all the above measurements, estimation, simulation, and fuzzy model development. A Performance regression plot was generated using MATLAB (training, testing, and validation) with the critical outputs of both fuzzy models (Grid impedance and Capacitor Lifetime) as shown in Fig. 12 additionally to justify the outcome of this investigation.

Fuzzy logic in MATLAB serves as a comprehensive tool for estimation, verification, and determination of critical parameters like grid impedance, capacitor lifetime, and their performance in this investigation. The fuzzy logic model is developed with a well-defined linguistic variable definition, parameters and their range, membership functions, and a fuzzy rule interface system. One of the proven and suitable defuzzification techniques is selected to estimate the desired fuzzy output in line with measured or estimated values of critical parameters. Fuzzy logic supports all intermediate output values and trend determination which is an alternative to measurements or simulation over the entire range. Error, accuracy, root mean square variance determination, and comparison versus respective measured data points justify the performance of the fuzzy logic model.

IX. CONCLUSION

A detailed study on grid impedance (measurement and estimation) and its reliability impact on DC capacitors in VFD is the major contribution of this research investigation. Grid impedance and short circuit capacity (kA) were measured offline before testing in all these grid configurations. Grid impedance was observed to impact significantly input rectifier peak and RMS current, input voltage, and current distortion with a 250 kW VFD tested under different grid configurations and loading conditions. A detailed analytical evaluation of grid impedance/short circuit current was also done using recommended international procedure by Cooper Bussmann for various grid configurations. It was observed that both testing and analytical evaluation of grid impedance were in-line with acceptable tolerance. The simulation model was developed using Matlab Simulink for various grid configurations with the measured grid impedances. Comparisons between measurements and simulation revealed that the increase of grid short circuit (kA) of various grid configurations increased VFD input THD_i, RMS, and peak current. DC capacitor lifetime was observed increasingly impacted due to increased RMS and peak current. Results reveal that DC capacitor lifetime is reduced to 64873 hours (250 kW at 100 kA grid capacity) as against 112754 hours (Bay A, 250 kW). Dynamic online grid impedance estimation and implementation proposal within VFD has been discussed and justification/verification is done. A simple fuzzy model

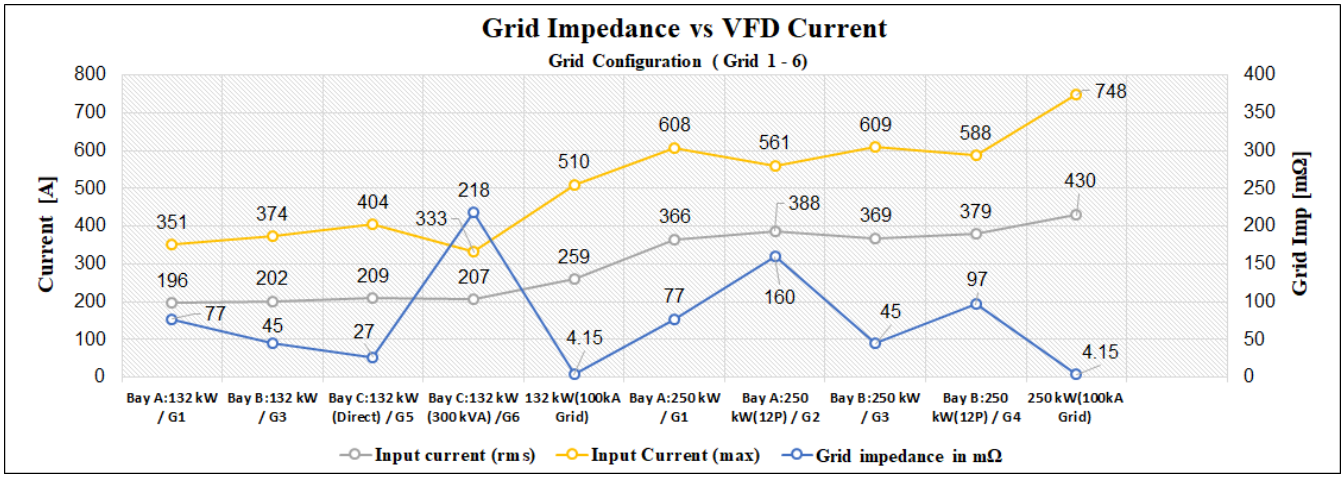

FIGURE 13. Measurement result: Grid impedance versus VFD current with different grid configurations at 415 V balanced supply condition.

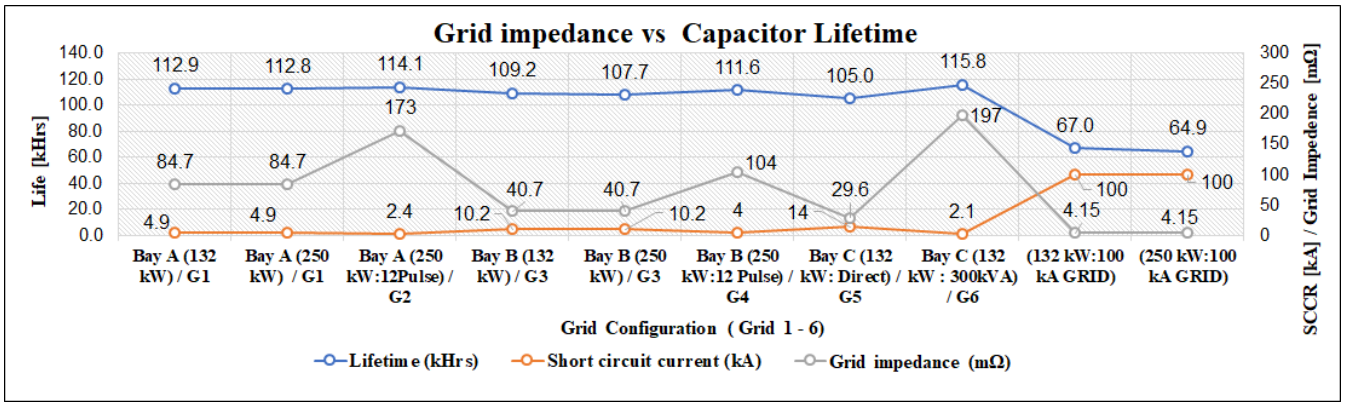

FIGURE 14. Grid impedance, Short circuit current (kA) versus Capacitor lifetime with different grid configuration.

for estimating grid impedance and capacitor lifetime was developed through MATLAB using measurements, simulation, and analysis results and observed to have an accuracy of 78.5% and 85.4% respectively. Reliability analysis of VFD (Predictive model) is also an additional outcome of this research investigation. This research proposal is an initial step toward built-in online grid impedance implementation in VFD which can be further enhanced across various aspects in future investigation.

As a future improvement of this investigation, a more dynamic, accurate, instantaneous, and large data sampling model for grid impedance estimation can be developed through advanced machine learning algorithms.

REFERENCES

[1] *IEEE Recommended Practice and Requirements for Harmonic Control in Electric Power Systems*, IEEE Standard 519-2014, Mar. 2014.

[2] *Electromagnetic Compatibility (EMC)—Part 3–2: Limits—Limits for Harmonic Current Emissions (Equipment Input Current ≤ 16 A Per Phase*, 5th ed., Standard IEC 61000-3-2:2018, Aug. 2021.

[3] *Electromagnetic Compatibility (EMC)—Part 3–12: Limits—Limits for Harmonic Current Produced by Equipment Connected to Public Low-Voltage Systems With Input Current > 16 A and ≤ 75 A Per Phase*, 2nd ed., Standard IEC 61000-3-12:2011, Jun. 2021.

[4] J. P. Rhode, A. W. Kelley, and M. E. Baran, "Complete characterization of utilization-voltage power system impedance using wideband measurement," *IEEE Trans. Ind. Appl.*, vol. 33, no. 6, pp. 1472–1479, Nov./Dec. 1997.

[5] A. Knop and F. W. Fuchs, "High frequency grid impedance analysis by current injection," in *Proc. 35th Annu. Conf. IEEE Ind. Electron.*, Nov. 2009, pp. 536–541.

[6] S. Cobreces, E. J. Bueno, D. Pizarro, F. J. Rodriguez, and F. Huerta, "Grid impedance monitoring system for distributed power generation electronic interfaces," *IEEE Trans. Instrum. Meas.*, vol. 58, no. 9, pp. 3112–3121, Sep. 2009.

[7] M. Jordan, H. Langkowski, T. D. Thanh, and D. Schulz, "Frequency dependent grid-impedance determination with pulse-width-modulation-signals," in *Proc. 7th Int. Conf., Workshop Compat. Power Electron. (CPE)*, Jun. 2011, pp. 131–136.

[8] M. Ciobotaru, R. Teodorescu, and F. Blaabjerg, "On-line grid impedance estimation based on harmonic injection for grid-connected PV inverter," in *Proc. IEEE Int. Symp. Ind. Electron.*, Jun. 2007, pp. 2437–2442.

[9] M. Cespedes and J. Sun, "Online grid impedance identification for adaptive control of grid-connected inverters," in *Proc. IEEE Energy Convers. Congr. Expo. (ECCE)*, Sep. 2012, pp. 914–921.

[10] D. Chakravorty, J. Meyer, P. Schegner, S. Yanchenko, and M. Schocke, "Impact of modern electronic equipment on the assessment of network harmonic impedance," *IEEE Trans. Smart Grid*, vol. 8, no. 1, pp. 382–390, Jan. 2017.

[11] L. Jessen, S. Gunter, F. W. Fuchs, M. Gottschalk, and H.-J. Hinrichs, "Measurement results and performance analysis of the grid impedance in different low voltage grids for a wide frequency band to support grid integration of renewables," in *Proc. IEEE Energy Convers. Congr. Expo. (ECCE)*, Sep. 2015, pp. 1960–1967.

[12] A. Vijayakumari, A. T. Devarajan, and N. Devarajan, "Decoupled control of grid connected inverter with dynamic online grid impedance measurements for micro grid applications," *Int. J. Electr. Power Energy Syst.*, vol. 68, pp. 1–14, Jun. 2015.

[13] Cooper Bussmann. *Short-Circuit Calculations*. Accessed: Mar. 22, 2020. [Online]. Available: https://www.eaton.com/content/dam/eaton/products/electrical-circuit-protection/fuses/solution-center/bus-ele-tech-lib-electrical-formulas.pdf

[14] M. Domagk, R. Stiegler, and J. Meyer, "Measurement based identification of equivalent circuit models for aggregated harmonic impedances of public low voltage grids," in *Proc. IEEE Milan PowerTech*, Jun. 2019, pp. 1–6, doi: 10.1109/PTC.2019.8810496.

[15] *METREL Euro Z800V MI3144 Manual*. Accessed: Mar. 22, 2020. [Online]. Available: https://www.metrel.si/assets/Metrel/Navodila_instrumentov/Instruments/MI_3144_Euro_Z_800V/Ang/MI_3144_Euro_Z_800_V_ANG_Ver_1.3.3_20752881.pdf

[16] S. Babaev, S. Cobben, V. Ćuk, and H. van den Brom, "Online estimation of cable harmonic impedance in low-voltage distribution systems," *IEEE Trans. Instrum. Meas.*, vol. 69, no. 6, pp. 2779–2789, Jun. 2020, doi: 10.1109/TIM.2019.2926690.

[17] M. B. A. Shuvho, M. A. Chowdhury, S. Ahmed, and M. A. Kashem, "Prediction of solar irradiation and performance evaluation of grid connected solar 80 KWp PV plant in Bangladesh," *Energy Rep.*, vol. 5, pp. 714–722, Nov. 2019.

[18] R. Pandurangan, P. Kaliannan, and P. Shanmugam, "Effects of current distortion on DC link inductor and capacitor lifetime in variable frequency drive connected to grid with active harmonic filter," *IEEE Trans. Ind. Appl.*, vol. 57, no. 1, pp. 492–505, Jan./Feb. 2021.

[19] *United Chemi-Con*. Accessed: Mar. 22, 2020. [Online]. Available: http://www.chemi-con.com/education/CapacitorLife

[20] A. Robert, "Guide for assessing the network harmonic impedance," in *Proc. 14th Int. Conf. Exhib. Electr. Distrib. Contrib.*, vol. 2, 1997, p. 310, doi: 10.1049/cp:19970473.

[21] W. Huai and F. Blaabjerg, "Reliability of capacitors for DC-link applications in power electronic converters—An overview," *IEEE Trans. Ind. Appl.*, vol. 50, no. 5, pp. 3569–3578, Sep./Oct. 2014, doi: 10.1109/TIA.2014.2308357.

RAMESH PANDURANGAN received the Diploma degree in electronics and communication engineering from Government Polytechnic, Coimbatore, India, in 1985, the bachelor's degree in electronics and communication engineering from the Government College of Technology, Coimbatore, in 1991, and the master's degree in electrical and electronics engineering with specialization in applied electronics from the PSG College of Technology, Coimbatore, in 1997. He is currently pursuing the Ph.D. degree in electrical engineering with the Vellore Institute of Technology, Vellore, India. He was associated with Product Management and Development of Drives Segment, Danfoss Industries Pvt. Ltd., Oragadam, India. He is one of the inventors of international patents in a screw compressor control system.

PALANISAMY KALIANNAN (Senior Member, IEEE) received the B.E. degree in electrical engineering from the KSR College of Technology, Tiruchengode, India, in 2000, the master's degree (Hons.) in applied electronics from the Coimbatore Institute of Technology, Coimbatore, India, in 2004, and the Ph.D. degree in electrical engineering from the Vellore Institute of Technology, Vellore, India, in 2013.

From 2016 to 2018, he was the Head of the Department of Energy and Power Electronics Division. He has been currently an Associate Professor of Energy and Power Electronics Division and the Head of the Centre for Smart Grid Technology, Vellore Institute of Technology, since 2007. He has authored more than 96 scientific papers in refereed conference proceedings and internal journals in the field of renewable energy, battery energy storage, multilevel converters, and power quality. He is a certified Energy Auditor by the Bureau of Energy Efficiency, Government of India. He has taken up various consultancy projects in energy efficiency and power quality improvement.

PARAMASIVAM SHANMUGAM (Senior Member, IEEE) received the B.E. degree from the Government College of Technology, Coimbatore, India in 1995, the M.E. degree from the PSG College of Technology Coimbatore, India, in 1999, and the Ph.D. degree in electrical engineering from the College of Engineering, Anna University, Chennai, India, in 2006.

He is currently with ESAB Research and Development Engineering Services Division. He has authored or coauthored more than 150 papers on various aspects of SRM and induction motor drives in international journals and conferences worldwide. He has been associated with various international journals on different editorial activities. His research interests include power electronics, ac motor drives, DSP and FPGA based motor controls, power factor correction, magnetic design, fuzzy logic, neural networks, and controller design for wind energy conversion systems.